

 Open access • Journal Article • DOI:10.1021/ACSNANO.5B03308

Two-Photon Absorption in Organometallic Bromide Perovskites — [Source link](#)

[Grant Walters](#), [Brandon R. Sutherland](#), [Sjoerd Hoogland](#), [Dong Shi](#) ...+4 more authors

Institutions: [University of Toronto](#), [King Abdullah University of Science and Technology](#)

Published on: 27 Jul 2015 - [ACS Nano](#) (American Chemical Society)

Topics: [Two-photon absorption](#), [Photoluminescence](#), [Trihalide](#), [Absorption \(electromagnetic radiation\)](#) and [Band gap](#)

Related papers:

- [Low trap-state density and long carrier diffusion in organolead trihalide perovskite single crystals](#)
- [Lead halide perovskite nanowire lasers with low lasing thresholds and high quality factors](#)
- [Nonlinear Absorption and Low-Threshold Multiphoton Pumped Stimulated Emission from All-Inorganic Perovskite Nanocrystals](#)
- [Low-temperature solution-processed wavelength-tunable perovskites for lasing](#)
- [Nanocrystals of Cesium Lead Halide Perovskites \(CsPbX₃, X = Cl, Br, and I\): Novel Optoelectronic Materials Showing Bright Emission with Wide Color Gamut](#)

Share this paper:    

View more about this paper here: <https://typeset.io/papers/two-photon-absorption-in-organometallic-bromide-perovskites-3gkbuvdsd>

ACS NANO

Article



ACS Nano is published
by the American
Chemical Society, 1155
Sixteenth Street N.W.,
Washington, DC 20036

ACS Publications

Published by American
Chemical Society.

Copyright © American
Chemical Society.

However, no copyright

ACS NANO

~~Two-Photon~~

Absorption in

ACS Publications



ACS Nano is published
by the American
Chemical Society, 1155
Sixteenth Street N.W.,
Washington, DC 20036

Published by American
Chemical Society.

Copyright © American
Chemical Society.

However, no copyright

ACS NANO

Organometallic

Bromide Perovskites



ACS Nano is published
by the American
Chemical Society, 1155
Sixteenth Street N.W.,
Washington, DC 20036

Published by American
Chemical Society.

Copyright © American
Chemical Society.

However, no copyright

ACS NANO

Grant Walters, Brandon R
Sutherland, Sjoerd Hoogland,
Dong Shi, Riccardo Comin,



ACS Nano is published
by the American
Chemical Society, 1155
Sixteenth Street N.W.,
Washington, DC 20036

ACS Publications

Published by American
Chemical Society.

Copyright © American
Chemical Society.

However, no copyright

ACS NANO

Daniel P. Sellan, Osman M. Bakr, and Edward H. Sargent



ACS Publications

ACS Nano is published
by the American
Chemical Society, 1155
Sixteenth Street N.W.,
Washington, DC 20036

Published by American
Chemical Society.

Copyright © American
Chemical Society.

However, no copyright

ACS NANO

ACS Nano, **Just Accepted**
Manuscript • DOI: 10.1021/



ACS Nano is published
by the American
Chemical Society, 1155
Sixteenth Street N.W.,
Washington, DC 20036

ACS Publications

Published by American
Chemical Society.

Copyright © American
Chemical Society.

However, no copyright

ACS NANO

acsnano.5b03308 • Publication
Date (Web): 21 Jul 2015



ACS Nano is published
by the American
Chemical Society. 1155
Sixteenth Street N.W.,
Washington, DC 20036

ACS Publications

Published by American
Chemical Society.

Copyright © American
Chemical Society.

However, no copyright

ACS NANO

Downloaded from <http://pubs.acs.org> on July 26, 2015



ACS Publications

ACS Nano is published
by the American
Chemical Society, 1155
Sixteenth Street N.W.,
Washington, DC 20036

Published by American
Chemical Society.

Copyright © American
Chemical Society.

However, no copyright

ACS NANO

Just Accepted



ACS Nano is published
by the American
Chemical Society. 1155
Sixteenth Street N.W.,
Washington, DC 20036

ACS Publications

Published by American
Chemical Society.

Copyright © American
Chemical Society.

However, no copyright

ACS NANO

“Just Accepted” manuscripts have been posted online prior to technical editing, formatting, and proofreading.



ACS Nano is published by the American Chemical Society, 1155 Sixteenth Street N.W., Washington, DC 20036

ACS Publications

Published by American Chemical Society.

Copyright © American Chemical Society.

However, no copyright

ACS NANO

Society provides "Just Accepted" as a
dissemination of scientific material as soon as possible after the
manuscript is accepted for publication. Just Accepted articles may
appear in full in PDF format accompanied by abstracts and
summaries.



ACS Publications

ACS Nano is published
by the American
Chemical Society, 1155
Sixteenth Street N.W.,
Washington, DC 20036

Published by American
Chemical Society.

Copyright © American
Chemical Society.

However, no copyright

ACS NANO

fully peer reviewed, but should not be considered
readers and citable by the Digital Object Identifier
to authors. Therefore, the Just Accepted



ACS Publications

ACS Nano is published
by the American
Chemical Society, 1155
Sixteenth Street N.W.,
Washington, DC 20036

Published by American
Chemical Society.

Copyright © American
Chemical Society.

However, no copyright

ACS NANO

in the journal. After a manuscript is technically accepted, it is posted on the "Manuscript Accepted" Web site and published as an article. Any changes to the manuscript text and/or graphics



ACS Publications

ACS Nano is published
by the American
Chemical Society, 1155
Sixteenth Street N.W.,
Washington, DC 20036

Published by American
Chemical Society.

Copyright © American
Chemical Society.

However, no copyright

ACS NANO

and ethical guidelines that apply to the
or consequences arising from the use of



ACS Nano is published
by the American
Chemical Society. 1155
Sixteenth Street N.W.,
Washington, DC 20036

Published by American
Chemical Society.

Copyright © American
Chemical Society.

However, no copyright



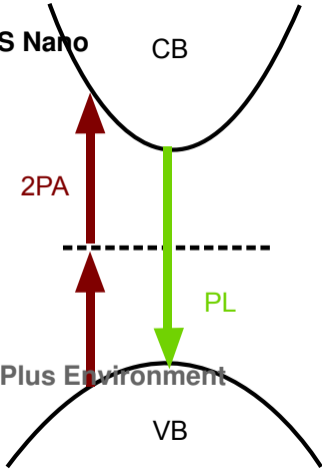
ACS Nano

CB

2PA

PL

VB



Two-Photon Absorption in Organometallic Bromide Perovskites

Grant Walters,^{1†} Brandon R. Sutherland,^{1†} Sjoerd Hoogland,¹ Dong Shi,² Riccardo Comin,¹ Daniel P. Sellan,¹ Osman M. Bakr,² Edward. H. Sargent^{1}*

¹ Department of Electrical and Computer Engineering, University of Toronto, Toronto, Ontario M5S 3G4, Canada

² Division of Physical Sciences and Engineering, Solar and Photovoltaics Engineering Research Center, King Abdullah University of Science and Technology (KAUST), Thuwal 23955-6900, Saudi Arabia

KEYWORDS: perovskite, $\text{CH}_3\text{NH}_3\text{PbBr}_3$, two-photon absorption, photoconductor, autocorrelator

ABSTRACT: Organometallic trihalide perovskites are solution processed semiconductors that have made great strides in third generation thin film light harvesting and light emitting optoelectronic devices. Recently it has been demonstrated that large, high purity single crystals of these perovskites can be synthesized from the solution phase. These crystals' large dimensions, clean bandgap, and solid-state order, have provided us with a suitable medium to observe and quantify two-photon absorption in perovskites. When $\text{CH}_3\text{NH}_3\text{PbBr}_3$ single crystals

1
2
3 are pumped with intense 800 nm light, we observe band-to-band photoluminescence at 572 nm,
4
5 indicative of two-photon absorption. We report the nonlinear absorption coefficient of
6
7 $\text{CH}_3\text{NH}_3\text{PbBr}_3$ perovskites to be 8.6 cm GW^{-1} at 800 nm, comparable to epitaxial single crystal
8
9 semiconductors of similar bandgap. We have leveraged this nonlinear process to electrically
10
11 autocorrelate a 100 fs pulsed laser using a two-photon perovskite photodetector. This work
12
13 demonstrates the viability of organometallic trihalide perovskites as a convenient and low-cost
14
15 nonlinear absorber for applications in ultrafast photonics.
16
17
18
19

20
21 Though formed at low temperature from the solution phase, organometallic halide perovskites
22
23 possess exceptional material properties. Perovskite thin films exhibit defect densities in the range
24
25 $10^{16} - 10^{17} \text{ cm}^{-3}$,¹ superior to other solution-cast semiconductors processed at similar
26
27 temperatures. Consistent with the low trap state density are the reported long and balanced
28
29 diffusion lengths,² large carrier mobilities,^{3,4} and a linear absorption coefficient exceeding 10^4
30
31 cm^{-1} at the band edge.⁵ Driven by these remarkable material properties, perovskite thin film
32
33 absorbers have demonstrated record solution-processed solar cell power conversion efficiencies
34
35 up to a certified 20.1%.⁶ Perovskite thin films have also been leveraged in light-emitting devices,
36
37 demonstrating low-threshold optically pumped lasers^{1,7,8} and high-brightness light-emitting
38
39 diodes.⁹
40
41
42
43
44

45
46 Recently, there have been breakthrough demonstrations of the solution-processed growth of
47
48 large perovskite single crystals.^{10,11} These single crystals offer millimeter-scale dimensions with
49
50 bulk trap state densities in the range $10^9 - 10^{10} \text{ cm}^{-3}$, comparable to some of the best epitaxial
51
52 single crystal semiconductors. The impressive energetic landscape in perovskite single crystals
53
54 has already been functionalized into ultra-low threshold optically pumped lasers.^{12,13}
55
56
57
58
59
60

1
2
3 We sought to investigate the two-photon absorption in $\text{CH}_3\text{NH}_3\text{PbBr}_3$ perovskites and to
4 demonstrate its potential in low-cost solution processed nonlinear optics. In addition to the
5 importance of understanding the response of organometallic hybrid perovskites under intense
6 radiation, their development as nonlinear optical materials and devices is a new opportunity.¹⁴
7
8 Semiconductor nonlinear absorbers have applications in optical limiting,¹⁵ characterization of
9 ultrafast optical signals,¹⁶ lithography,¹⁷ and microscopy.¹⁸
10
11
12
13
14
15
16
17

18 Equipped with the newly-discovered process to grow large single crystals, we were able to
19 overcome many existing experimental challenges associated with quantifying two-photon
20 absorption. We hypothesized that the large dimensions of single crystals, as well as their ultra-
21 clean bandgaps and long range order would be an ideal material to study perovskite two-photon
22 absorption. The small path length and dominant scattering of conventional perovskite thin films,
23 which proved to limit the accuracy of these measurements, would no longer be an issue. Here we
24 present an accurate quantification of two-photon absorption in $\text{CH}_3\text{NH}_3\text{PbBr}_3$. We demonstrate
25 its applicability in nonlinear optics by autocorrelating a 100 fs laser using a perovskite two
26 photon photodetector. This work is the first report of two-photon absorption and autocorrelation
27 from a solution-processed single crystal organic-inorganic semiconductor.
28
29
30
31
32
33
34
35
36
37
38
39
40
41
42

43 RESULTS AND DISCUSSION

44
45

46 To study $\text{CH}_3\text{NH}_3\text{PbBr}_3$ perovskite, we employed the same vapor-assisted single crystal
47 growth technique reported by Shi *et al.*¹⁰ Here, the gradual diffusion of an antisolvent into a
48 solution of perovskite precursors promotes seed formation and subsequent crystal growth. The
49 resulting crystals are orange in color with regular rectangular facets (see Figure 1a inset). The
50 large dimensions of the crystals we used enabled accurate measurements of two-photon
51
52
53
54
55
56
57
58
59
60

1
2
3 absorption, the magnitude of which is directly impacted by the propagation distance through the
4
5 sample.
6
7

8
9 Two-photon absorption is a third-order nonlinear process that becomes relevant at high photon
10
11 fluences. Two photons, each with energy less than the difference between the material's ground
12
13 and excited states, are simultaneously absorbed and excite a charge carrier. In semiconductors,
14
15 this is manifested as an excitation across the bandgap. Two-photon absorption varies with the
16
17 square of the electric field intensity I . The attenuation of light propagating a distance z through a
18
19 two-photon absorbing medium can thus be written as,
20
21

$$\frac{dI}{dz} = -\alpha I - \beta I^2, \quad (1)$$

22
23
24 where α and β are the one- (linear) and two-photon absorption coefficients respectively. The
25
26 solution of this differential equation, expressing the transmission T through a sample of length L ,
27
28 is:
29
30
31
32
33

$$T = \frac{I}{I_0} = \frac{e^{-\alpha L}}{\beta I_0 L_{eff} + 1}, \quad (2)$$

34
35
36 where I_0 is the peak intensity of light entering the sample and L_{eff} is the effective sample length
37
38 given by,
39
40
41
42
43
44

$$L_{eff} = \frac{1 - e^{-\alpha L}}{\alpha}. \quad (3)$$

45
46
47 The intensity of light entering the sample is found by reducing the measured incident intensity by
48
49 a factor of $(1 - R)$ where R is the surface reflectivity.
50
51
52
53
54
55
56
57
58
59
60

1
2
3 In order to achieve degenerate two-photon absorption in our samples we used a high-power
4 mode-locked titanium sapphire laser operating at 800 nm to provide below-bandgap excitation.
5
6 The bandgap of $\text{CH}_3\text{NH}_3\text{PbBr}_3$ is 2.21 eV,¹⁰ with an absorption onset at 560 nm as shown in
7
8 Figure 1a. This onset is sharp, leading to nearly constant absorption for above-bandgap radiation.
9
10 The step-like behavior in the absorption ensured the samples were free from linear absorption of
11
12 the incident laser light. Previous transient absorption measurements on $\text{CH}_3\text{NH}_3\text{PbBr}_3$ single
13
14 crystals using above-bandgap pump and below-bandgap probe lasers have shown significant
15
16 changes in optical absorption within picoseconds of excitation; however, the excited population
17
18 that allows for this change in absorption quickly decays such that the material regains its below-
19
20 bandgap transparency within nanoseconds.¹⁰ We have used ultra-short pulses (100 fs) with a
21
22 periodicity of 13 ns in our experiments. The use of ultra-short pulses in our experiments and the
23
24 absence of linear absorption means photoinduced absorption associated with excited-state
25
26 carriers was negligible and did not affect the accuracy of our measurements.
27
28
29
30
31
32
33
34

35 Strikingly bright green light is visibly emitted when the samples are placed in the path of the
36
37 laser (Figure 1a inset). This photoluminescence was direct evidence that our samples were in-fact
38
39 absorbing the below-bandgap 800 nm radiation through two-photon absorption. The resulting
40
41 emission spectrum in Figure 1a shows a sharp and narrow peak at 572 nm—with a wavelength
42
43 dependence unchanged from linearly induced photoluminescence. Thus the perovskite crystals
44
45 behave as an effective upconverter for near infrared radiation. A simple schematic of the two-
46
47 photon absorption and induced photoluminescence process is given in Figure 1b.
48
49
50
51

52 The z-scan procedure¹⁹ is the most widely-used method for measuring two-photon absorption
53
54 coefficients because of its simplicity and ease of data interpretation. It involves translating the
55
56 sample along the path of a focused laser beam in order to vary the incident intensity and find β .
57
58
59
60

1
2
3 Although convenient, the method can be prone to artefacts and overestimation with less-than-
4 ideal samples. To avoid possible changes in scattering associated with changes in the spot-size as
5 the sample is translated for z-scans, we opted to alternatively measure the two-photon absorption
6 coefficient for $\text{CH}_3\text{NH}_3\text{PbBr}_3$ through static intensity-dependent transmission measurements.
7
8 This straight-forward technique provides an accurate description of two-photon absorption
9 behavior.²⁰ These measurements were made by placing the sample at the waist of the focused
10 laser beam, varying the laser intensity with a filter wheel, and monitoring incident and
11 transmitted power.
12
13
14
15
16
17
18
19
20
21
22

23 A typical plot of inverse transmission *versus* peak intensity is given in Figure 2a. The plot
24 shows the requisite linear increase with intensity according to equation 2 accompanied by an
25 expected slight downward curvature, the latter behavior indicating temporal and spatial
26 broadening of the beam towards the rear of the sample when subjected to high intensities.²⁰ The
27 solid line is a least-squares fit according to the equations for temporally and spatially Gaussian
28 pulses developed by Sheik-Bahae *et al.*¹⁹:
29
30
31
32
33
34
35
36
37

$$T(I_0) = \sum_{m=0}^{\infty} \frac{[-q(I_0)]^m}{(m+1)^{\frac{3}{2}}}, \quad (4)$$

$$q(I_0) = \beta I_0 L_{eff}, \quad (5)$$

38
39
40
41
42
43
44
45
46
47 The sum in equation 4 was performed for 20 terms to ensure proper convergence of the function.
48
49 Although linear absorption can be ignored for these samples, they often showed significant
50 scattering and so this loss mechanism was treated as linear absorption in accordance with Ref.²⁰.
51
52 Repeated measurements on several samples yielded an average absorption coefficient of $8.6 \pm$
53
54
55
56
57
58
59
60
61
62
63
64
65
66
67
68
69
70
71
72
73
74
75
76
77
78
79
80
81
82
83
84
85
86
87
88
89
90
91
92
93
94
95
96
97
98
99
100
101
102
103
104
105
106
107
108
109
110
111
112
113
114
115
116
117
118
119
120
121
122
123
124
125
126
127
128
129
130
131
132
133
134
135
136
137
138
139
140
141
142
143
144
145
146
147
148
149
150
151
152
153
154
155
156
157
158
159
160
161
162
163
164
165
166
167
168
169
170
171
172
173
174
175
176
177
178
179
180
181
182
183
184
185
186
187
188
189
190
191
192
193
194
195
196
197
198
199
200
201
202
203
204
205
206
207
208
209
210
211
212
213
214
215
216
217
218
219
220
221
222
223
224
225
226
227
228
229
230
231
232
233
234
235
236
237
238
239
240
241
242
243
244
245
246
247
248
249
250
251
252
253
254
255
256
257
258
259
260
261
262
263
264
265
266
267
268
269
270
271
272
273
274
275
276
277
278
279
280
281
282
283
284
285
286
287
288
289
290
291
292
293
294
295
296
297
298
299
300
301
302
303
304
305
306
307
308
309
310
311
312
313
314
315
316
317
318
319
320
321
322
323
324
325
326
327
328
329
330
331
332
333
334
335
336
337
338
339
340
341
342
343
344
345
346
347
348
349
350
351
352
353
354
355
356
357
358
359
360
361
362
363
364
365
366
367
368
369
370
371
372
373
374
375
376
377
378
379
380
381
382
383
384
385
386
387
388
389
390
391
392
393
394
395
396
397
398
399
400
401
402
403
404
405
406
407
408
409
410
411
412
413
414
415
416
417
418
419
420
421
422
423
424
425
426
427
428
429
430
431
432
433
434
435
436
437
438
439
440
441
442
443
444
445
446
447
448
449
450
451
452
453
454
455
456
457
458
459
460
461
462
463
464
465
466
467
468
469
470
471
472
473
474
475
476
477
478
479
480
481
482
483
484
485
486
487
488
489
490
491
492
493
494
495
496
497
498
499
500
501
502
503
504
505
506
507
508
509
510
511
512
513
514
515
516
517
518
519
520
521
522
523
524
525
526
527
528
529
530
531
532
533
534
535
536
537
538
539
540
541
542
543
544
545
546
547
548
549
550
551
552
553
554
555
556
557
558
559
560
561
562
563
564
565
566
567
568
569
570
571
572
573
574
575
576
577
578
579
580
581
582
583
584
585
586
587
588
589
590
591
592
593
594
595
596
597
598
599
600
601
602
603
604
605
606
607
608
609
610
611
612
613
614
615
616
617
618
619
620
621
622
623
624
625
626
627
628
629
630
631
632
633
634
635
636
637
638
639
640
641
642
643
644
645
646
647
648
649
650
651
652
653
654
655
656
657
658
659
660
661
662
663
664
665
666
667
668
669
670
671
672
673
674
675
676
677
678
679
680
681
682
683
684
685
686
687
688
689
690
691
692
693
694
695
696
697
698
699
700
701
702
703
704
705
706
707
708
709
710
711
712
713
714
715
716
717
718
719
720
721
722
723
724
725
726
727
728
729
730
731
732
733
734
735
736
737
738
739
740
741
742
743
744
745
746
747
748
749
750
751
752
753
754
755
756
757
758
759
760
761
762
763
764
765
766
767
768
769
770
771
772
773
774
775
776
777
778
779
780
781
782
783
784
785
786
787
788
789
790
791
792
793
794
795
796
797
798
799
800
801
802
803
804
805
806
807
808
809
810
811
812
813
814
815
816
817
818
819
820
821
822
823
824
825
826
827
828
829
830
831
832
833
834
835
836
837
838
839
840
841
842
843
844
845
846
847
848
849
850
851
852
853
854
855
856
857
858
859
860
861
862
863
864
865
866
867
868
869
870
871
872
873
874
875
876
877
878
879
880
881
882
883
884
885
886
887
888
889
890
891
892
893
894
895
896
897
898
899
900
901
902
903
904
905
906
907
908
909
910
911
912
913
914
915
916
917
918
919
920
921
922
923
924
925
926
927
928
929
930
931
932
933
934
935
936
937
938
939
940
941
942
943
944
945
946
947
948
949
950
951
952
953
954
955
956
957
958
959
960
961
962
963
964
965
966
967
968
969
970
971
972
973
974
975
976
977
978
979
980
981
982
983
984
985
986
987
988
989
990
991
992
993
994
995
996
997
998
999
1000

1
2
3 CdSe ($E_g = 1.74$ eV) have absorption coefficients of 5.5 cm GW^{-1} (at 530 nm) and 18 cm GW^{-1}
4 (at 1060 nm) respectively.²¹ The dependence of two-photon absorption with band-gap for
5
6
7
8
9
10
11
12
13
14
15
16
17
18
19
20
21
22
23
24
25
26
27
28
29
30
31
32
33
34
35
36
37
38
39
40
41
42
43
44
45
46
47
48
49
50
51
52
53
54
55
56
57
58
59
60

CdSe ($E_g = 1.74$ eV) have absorption coefficients of 5.5 cm GW^{-1} (at 530 nm) and 18 cm GW^{-1} (at 1060 nm) respectively.²¹ The dependence of two-photon absorption with band-gap for semiconductors is well established and we find our value for $\text{CH}_3\text{NH}_3\text{PbBr}_3$ agrees well with the reported scaling laws.^{20–22} The experimental value has only a 14% error with our own prediction based on these relations: 10 cm GW^{-1} . Consideration of the corresponding scaling laws for the nonlinear refractive index and the Kramers-Kronig relation between the two-photon absorption coefficient and the nonlinear refractive index shows that the nonlinear reflection due to changes in the material's refractive index (a maximum change of 10^{-5}) is negligible and does not impact the measured two-photon absorption coefficient.²²

The use of single crystals enabled us to measure the polarization dependence of two-photon absorption in the perovskites. These measurements are fundamentally impossible with polycrystalline thin films due to their random lattice orientations. Figure 2b shows the polarization dependence of two-photon absorption for $\text{CH}_3\text{NH}_3\text{PbBr}_3$. Plotted is the transmission scaled by the incident intensity T/I_{in} – a quantity directly proportional to the absorption coefficient. A half-wave plate was used to rotate the incident beam's electric field polarization an angle θ relative to the [100] crystallographic axis and the incident propagation along the [001] direction such that the polarization rotated through the crystallographic xy plane. $\text{CH}_3\text{NH}_3\text{PbBr}_3$ is cubic with the space group $P m\bar{3}m$ at room temperature,¹⁰ and so the polarization dependence can be modeled with:

$$\frac{T}{I_{in}} = A[1 + 2\sigma[\sin^4(\theta + \varphi) - \sin^2(\theta + \varphi)]], \quad (6)$$

1
2
3 where A is related to the imaginary component of the susceptibility tensor element $\chi_{xxxx}^{(3)}$, σ is
4 the sample anisotropy parameter, and φ is the wave-plate angular offset.^{23–25} A least-squares fit
5
6 is shown in Figure 2b and yields an anisotropy parameter of $\sigma = -0.07$.
7
8
9

10
11 $\text{CH}_3\text{NH}_3\text{PbBr}_3$ and other organometallic perovskites have previously been predicted, through
12 density functional theory calculations, to exhibit a large spin-orbit coupling due to the heavy lead
13 atoms.^{26–31} This coupling splits the degenerate conduction band, such that a doublet band is
14 lowered and a quartet band is raised in energy.²⁶ These predictions are supported by an
15 agreement between the experimentally measured and the predicted values for the bandgap. For
16 semiconductors in general, the valence band to lowest conduction band transitions do not provide
17 any orientational dependence for two-photon absorption.^{24,25,32} Anisotropic behavior may be
18 introduced either from direct transitions between the valence bands and the higher conduction
19 bands or from state mixing between these bands.^{24,25,32} These mechanisms are minimal in
20 $\text{CH}_3\text{NH}_3\text{PbBr}_3$ where the conduction bands have a large energetic separation, consistent with the
21 small anisotropy parameter observed.
22
23
24
25
26
27
28
29
30
31
32
33
34
35
36
37
38

39 We utilized the nonlinear properties of our perovskite single crystals for autocorrelation
40 purposes. This can be done with measurements of the nonlinear response of transmission,
41 photoluminescence intensity, second harmonic generation, or electrical current. In line with the
42 facile processing of the perovskite crystals and their exceptional electrical properties we aimed to
43 use electrical current, one of the most straightforward signals to measure, as our autocorrelation
44 signal.
45
46
47
48
49
50
51
52
53

54 We fabricated a simple photoconductor by depositing silver contacts on opposite ends of a
55 single crystal. A schematic of the photodetector, along with the crystal dimensions is shown in
56
57
58
59
60

1
2
3 Figure 3a. The sample is illuminated from the side, resulting in single-pass two-photon
4 absorption of 800 nm light. The dark current-voltage characteristic of this crystal is shown in
5
6 Figure 3b. This crystal has an electrical conductivity of $10^{-5} \Omega^{-1} \text{ cm}^{-1}$.
7
8
9

10
11 The photocurrent (light minus dark current) generated as a result of single-pass absorption of
12 800 nm light is given as a function of peak intensity of the pump laser at a fixed bias of 50 V in
13 Figure 3c. We tested control samples of just glass and just silver and no photocurrent is
14 observed. Photoconductors based on linear absorption have a photocurrent which increases
15 sublinearly (power-law dependence $n < 1$) with input intensity (see Supporting Information
16 Figure S1a).³³ However, the two-photon absorption probability increases with the square of input
17 intensity ($n = 2$). We therefore expect a photocurrent dependence on input intensity which is less
18 than $n = 2$, but greater than linear photoconduction ($n < 1$), which is what we observe.
19
20
21
22
23
24
25
26
27
28
29
30

31 The responsivity (efficiency in A W^{-1}) of the two photon photodetector at a fixed bias of 50 V
32 as a function of input intensity is given in Figure 3d. The responsivity is of order 10^{-7} . This value
33 is five orders of magnitude less than the upper limit in the absence of photoconductive gain as
34 determined by the two-photon absorption coefficient. Low responsivity is expected given that
35 perovskites, with their low trap state density and balanced carrier mobilities, exhibit low intrinsic
36 photoconductive gain.³⁴ Despite the low gain, due to the large number of total absorbed photons,
37 the device output photocurrent is in the range 10 nA – 1 μA , readily measurable using a
38 conventional current meter. The responsivity increases 3.5x over 1 decade of input intensity.
39
40 This is contrary to linear photoconductors, which have a responsivity that decreases with
41 increasing input intensity (see Supporting Information Figure S1b). This upward trend
42 demonstrates that the photocurrent is a result of nonlinear absorption and not linear processes
43 such as thermal generation or trap-mediated absorption.
44
45
46
47
48
49
50
51
52
53
54
55
56
57
58
59
60

1
2
3 A schematic of our perovskite autocorrelator is shown in Figure 4a. A 100 fs, 800 nm pulse
4 passes through a 50/50 beam splitter (BS). One arm is sent to a retro-reflector on a delay line.
5
6 The two arms meet again at a second 50/50 splitter which sends half of the total light to a power
7
8 meter (det), the other half through a focusing lens onto the two-photon absorbing perovskite
9
10 photodetector. The generated photocurrent is collected using a current meter and monitored as a
11
12 function of the delay line position. The resulting current-time trace is shown in Figure 4b. Our
13
14 autocorrelator configuration is a modified Mach–Zehnder interferometer where the two pulses
15
16 have the same phase and polarization. With this configuration, we observe constructive and
17
18 destructive interference fringes corresponding to the overlap of the time-varying electrical fields.
19
20 The envelope of these fringes corresponds to the intensity overlap of the pulses in time. We fit
21
22 the top and bottom envelopes to a $\text{sech}^2(t)$ function, shown in red. The resulting autocorrelation
23
24 has a full-width at half-maximum (FWHM) of 160 fs. Since we are autocorrelating the electric
25
26 field, but we wish to know the intensity profile, there is a deconvolution factor to be applied. For
27
28 a $\text{sech}^2(t)$ input pulse intensity profile, the deconvolution factor is 0.65,³⁵ resulting in a measured
29
30 pulse duration of 104 fs. This is in excellent agreement with the 100 fs specification of our laser.
31
32 The fringe spacing, limited by the resolution of our motorized stage, is approximately every 3/2
33
34 of a wavelength, shown in Figure 4c.
35
36
37
38
39
40
41
42
43

44 CONCLUSION

45
46
47 This work demonstrates the prospects of perovskites as solution processed two-photon
48
49 absorbers for applications in nonlinear optics. With just readily available chemical precursors,
50
51 researchers can fabricate large single crystal two-photon absorbers to accurately and
52
53 conveniently autocorrelate ultrafast lasers. Yet, the nonlinear optical properties of perovskites
54
55 remain largely unexplored. Future work will focus on investigating new avenues for perovskites
56
57
58
59
60

1
2
3 as nonlinear optical materials, such as studying secondary harmonic generation, optical limiting,
4
5 and self-focusing.
6
7

8 9 METHODS

10
11
12 $\text{CH}_3\text{NH}_3\text{PbBr}_3$ single crystals were prepared using a vapor-assisted crystallization procedure as
13 previously reported.¹⁰ In brief, the vapor from an antisolvent (dichloromethane, in our case) was
14 allowed to slowly diffuse into a solution of perovskite precursors, lead bromide (PbBr_2) and
15 methylammonium bromide ($\text{CH}_3\text{NH}_3\text{Br}$) in N,N-dimethylformamide, such that precursors
16 spontaneously nucleated and co-crystallized in a self-sustained process. Crystals were kept in the
17 mother liquor until use in optical experiments. Their dimensions were measured using a
18 Mitutoyo digital caliper to within 10 μm .
19
20
21
22
23
24
25
26
27
28

29
30 Linear optical absorption was characterized using a PerkinElmer Lambda 950 UV/Vis/NIR
31 spectrophotometer in the wavelength range 250 – 900 nm and using 2 nm incremental steps.
32
33 Photoluminescence induced by linear absorption was measured using a Liconix Helium
34 Cadmium 442 nm excitation laser and Ocean Optics USB2000 spectrometer.
35
36
37
38

39
40 For all nonlinear absorption experiments, a mode-locked Mira 900-F Ti:Sapphire laser was
41 used as the excitation source. The pulse duration was 100 fs (FWHM) at a repetition rate of 76
42 MHz. The laser was tuned to an output wavelength of 800 nm and produced horizontally
43 polarized TEM_{00} -mode single pulses. Power measurements were made with an Ophir LaserStar
44 Dual Channel power and energy meter with photodiode sensors which had an accuracy of $\pm 5\%$
45 after attenuation at 800 nm.
46
47
48
49
50
51
52
53
54
55
56
57
58
59
60

1
2
3 Two-photon absorption coefficients were measured by placing the sample at the focus of a lens
4 with a 15 cm focal length and by attenuating the incident laser radiation with a neutral density
5 filter wheel. The incident and transmitted light was measured with power meters placed before
6 and after the sample. The lens focused the beam to a spot size of 35 μm (half-width at $1/e^2$) as
7 determined with a CCD camera setup. For most measurements, the incident beam was chopped
8 at 400 Hz in order to prevent sample heating and optical damage. To measure the polarization
9 dependence of two-photon absorption, a rotating half-wave plate was placed in the path of the
10 incident beam. Predicted absorption coefficients were determined through the scaling law,
11
12
13
14
15
16
17
18
19
20
21
22

$$\beta = 3100 \frac{\sqrt{E_P} (2\hbar\omega/E_g - 1)^{3/2}}{n^2 E_g^3 (2\hbar\omega/E_g)^5}, \quad (7)$$

23
24
25
26
27
28 where,

$$E_P = \frac{2P^2 m}{\hbar^2} \quad (\text{in eV}), \quad (8)$$

29
30
31
32 and E_g is the bandgap (eV), $\hbar\omega$ is the field energy (eV), m is the electron mass, n is the linear
33 refractive index (assumed 2.5) and P is the Kane momentum parameter (assumed 4.5×10^{-27} J
34 m).²⁰⁻²²
35
36
37
38
39
40
41
42
43

44 Photoconduction measurements were done using a device made from a single crystal with
45 wires bonded to opposing crystal faces with conductive silver paste. Two-photon absorption
46 photocurrent was measured using a Keithley 2410 High Voltage Source Meter (also used as a
47 bias source).
48
49
50
51
52
53

54 For autocorrelation experiments the incident laser beam was split into two branches, such that
55 a motorized translation stage with a retroreflector could be added to introduce a pulse-delay for
56
57
58
59
60

one of the paths. The separate paths were then rerouted into a single collinear path that was incident on our sample. Photocurrent was measured as a function of the retroreflector position in order to detect pulse-overlap and determine the autocorrelation width.

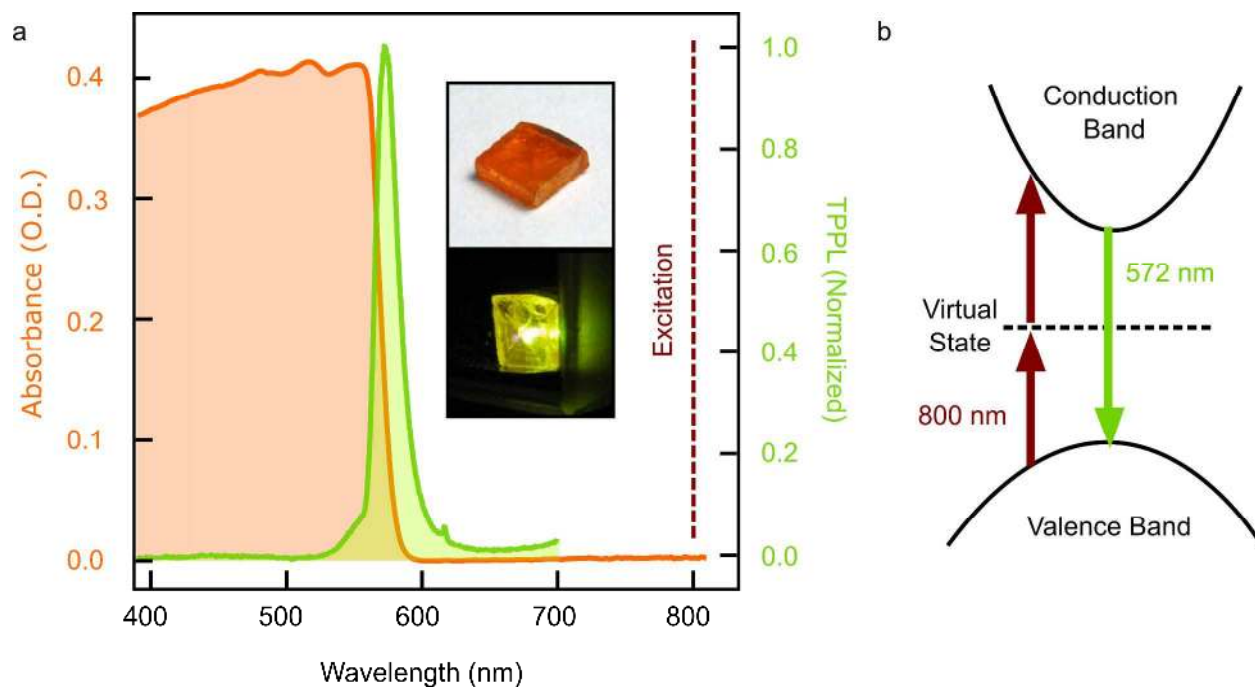


Figure 1. Optical properties. a) Linear optical absorbance (left axis) and normalized two-photon-induced photoluminescence (TPPL, right axis) as a function of wavelength for a single $\text{CH}_3\text{NH}_3\text{PbBr}_3$ crystal. Photoluminescence peaks at 572 nm. Insets show the crystal (dimensions $\sim 1 \times 5 \times 5$ mm) under room light (upper) and brightly luminescing when exposed to intense 800 nm laser radiation (lower). The visibly observed photoluminescence is a direct signature of two-photon absorption. b) Schematic showing two-photon absorption of 800 nm light and up-conversion to 572 nm photoluminescence.

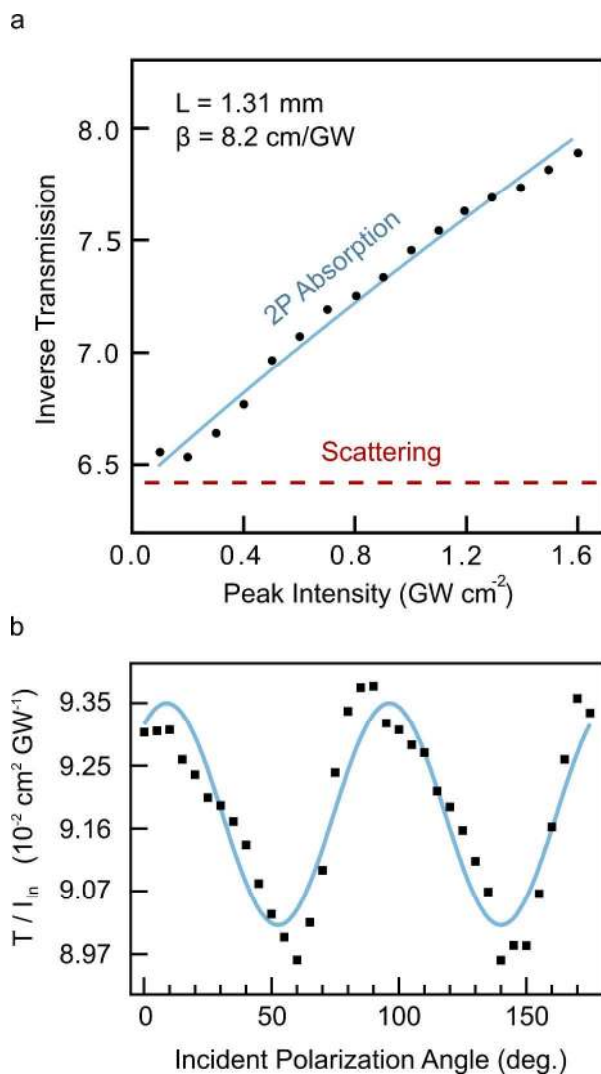


Figure 2. Two-photon absorption coefficient. a) Inverse transmission *versus* peak intensity for a typical single CH₃NH₃PbBr₃ crystal. The solid line is a least-squares fit to the data points using equations 4-5 resulting in a two-photon absorption coefficient of 8.2 GW cm⁻¹. Dashed red line indicates linear loss, primarily due to scattering. b) Transmission scaled by incident intensity *versus* electric field polarization angle relative [100] crystallographic axis (offset by 8 degrees). Solid line is a least-squares fit to equation 6 and yields an anisotropy parameter of -0.07.

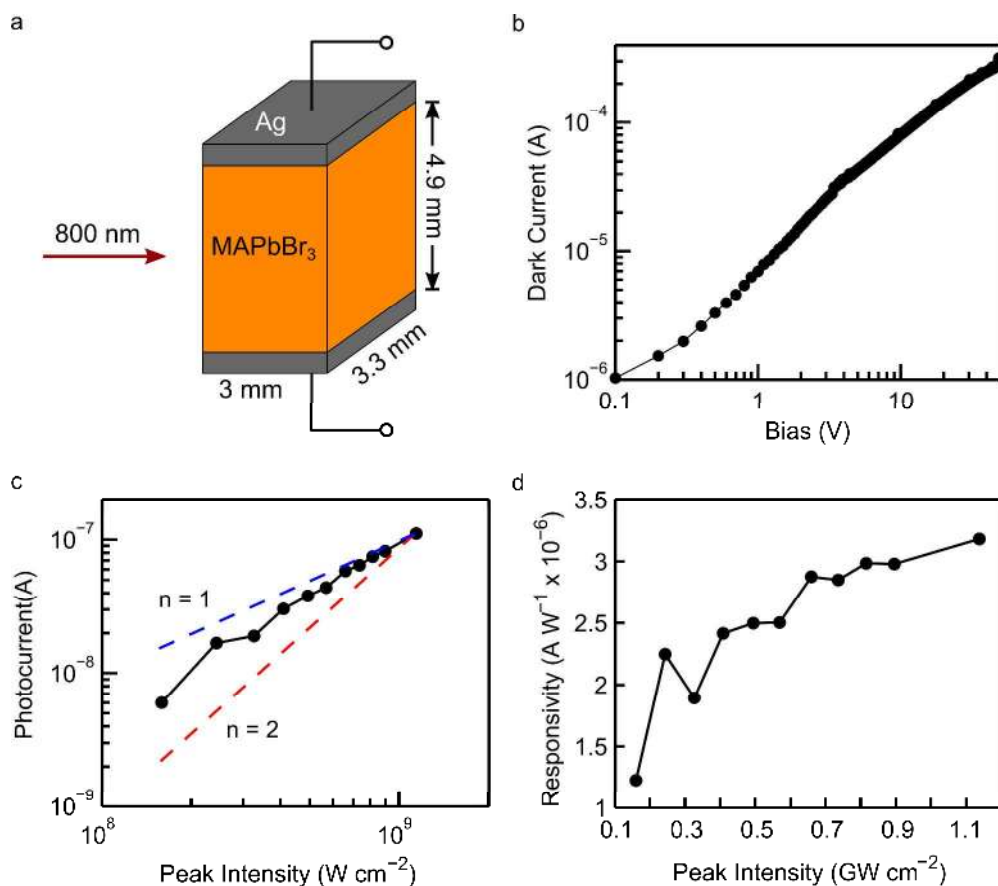


Figure 3. $\text{CH}_3\text{NH}_3\text{PbBr}_3$ two-photon photodetector. a) Device schematic. b) Dark current-voltage characteristic. The perovskite photoconductor has an electrical conductivity of order $10^{-5} \Omega^{-1} \text{ cm}^{-1}$. c) Net photocurrent (light current minus dark current) dependence on input light intensity at a bias of 50 V. The photodetector exhibits an intensity dependence which is a combination of two competing trends, the square ($n = 2$) dependence of two-photon absorption, and the sublinear ($n < 1$) dependence of photoconductive gain. d) Resistivity (photocurrent / input power) dependence on input intensity at a bias of 50 V. Contrary to linear photoconductors, the resistivity of the perovskite two-photon photoconductor does not decrease with increasing input intensity due to the squared dependence of absorption.

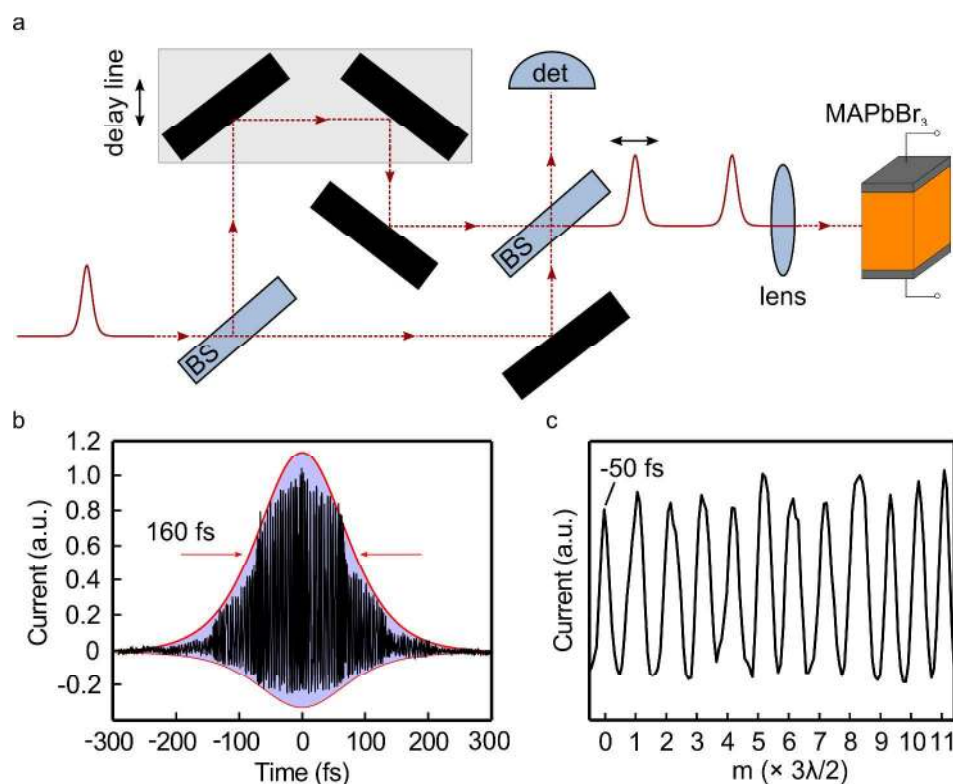


Figure 4. Autocorrelation of a 100 fs Ti:Sapphire laser using a $\text{CH}_3\text{NH}_3\text{PbBr}_3$ two-photon detector. a) Optical schematic. The input laser pulse is split into two, with one pulse variably delayed in time using a retroreflector on a motorized linear translation stage. Photocurrent generated by the two-photon perovskite photodetector is used to autocorrelate the beam pulse. b) Autocorrelation signal. We observe a 160 fs FWHM in the autocorrelation envelope, corresponding to a 100 fs pulse width. c) Electric field interference. We resolve constructive interference approximately every $3\lambda/2$.

1
2
3 ASSOCIATED CONTENT
4

5
6
7 **Supporting Information Available:** Photoconductor operating under above-bandgap
8
9 illumination. This material is available free of charge via the Internet at <http://pubs.acs.org>.
10
11

12
13
14 AUTHOR INFORMATION15
16
17 **Corresponding Author**

18
19 * Email: ted.sargent@utoronto.ca
20
21

22
23 **Author Contributions**

24
25 The manuscript was written through contributions of all authors. All authors have given approval
26
27 to the final version of the manuscript. †These authors contributed equally.
28
29

30
31 ACKNOWLEDGMENT

32
33
34 This publication is based in part on work supported by Award KUS-11-009-21, made by King
35
36 Abdullah University of Science and Technology (KAUST), by the Ontario Research Fund -
37
38 Research Excellence Program, and by the Natural Sciences and Engineering Research Council
39
40 (NSERC) of Canada.
41
42
43

44
45 REFERENCES

- 46
47 (1) Xing, G.; Mathews, N.; Lim, S. S.; Yantara, N.; Liu, X.; Sabba, D.; Grätzel, M.;
48 Mhaisalkar, S.; Sum, T. C. Low-Temperature Solution-Processed Wavelength-Tunable
49 Perovskites for Lasing. *Nat. Mater.* **2014**, *13*, 476–480.
50
51 (2) Xing, G.; Mathews, N.; Sun, S.; Lim, S. S.; Lam, Y. M.; Grätzel, M.; Mhaisalkar, S.; Sum,
52 T. C. Long-Range Balanced Electron-and Hole-Transport Lengths in Organic-Inorganic
53 CH₃NH₃PbI₃. *Science* **2013**, *342*, 344–347.
54
55 (3) Stoumpos, C. C.; Malliakas, C. D.; Kanatzidis, M. G. Semiconducting Tin and Lead
56 Iodide Perovskites with Organic Cations: Phase Transitions, High Mobilities, and Near-
57 Infrared Photoluminescent Properties. *Inorg. Chem.* **2013**, *52*, 9019–9038.
58
59
60

- 1
- 2
- 3
- 4 (4) Shao, Y.; Xiao, Z.; Bi, C.; Yuan, Y.; Huang, J. Origin and Elimination of Photocurrent Hysteresis by Fullerene Passivation in CH₃NH₃PbI₃ Planar Heterojunction Solar Cells. *Nat. Commun.* **2014**, *5*, 5784.
- 5
- 6
- 7 (5) Green, M. A.; Ho-Baillie, A.; Snaith, H. J. The Emergence of Perovskite Solar Cells. *Nat. Photonics* **2014**, *8*, 506–514.
- 8
- 9 (6) Yang, W. S.; Noh, J. H.; Jeon, N. J.; Kim, Y. C.; Ryu, S.; Seo, J.; Seok, S. I. High-Performance Photovoltaic Perovskite Layers Fabricated Through Intramolecular Exchange. *Science* **2015**, *348*, 1234–1237.
- 10
- 11
- 12 (7) Deschler, F.; Price, M.; Pathak, S.; Klintberg, L. E.; Jarausch, D.-D.; Högler, R.; Hüttner, S.; Leijtens, T.; Stranks, S. D.; Snaith, H. J.; *et al.* High Photoluminescence Efficiency and Optically Pumped Lasing in Solution-Processed Mixed Halide Perovskite Semiconductors. *J. Phys. Chem. Lett.* **2014**, *5*, 1421–1426.
- 13
- 14 (8) Sutherland, B. R.; Hoogland, S.; Adachi, M. M.; Wong, C. T. O.; Sargent, E. H. Conformal Organohalide Perovskites Enable Lasing on Spherical Resonators. *ACS Nano* **2014**, *8*, 10947–10952.
- 15
- 16 (9) Tan, Z.-K.; Moghaddam, R. S.; Lai, M. L.; Docampo, P.; Högler, R.; Deschler, F.; Price, M.; Sadhanala, A.; Pazos, L. M.; Credgington, D.; *et al.* Bright Light-Emitting Diodes Based on Organometal Halide Perovskite. *Nat. Nanotechnol.* **2014**, *9*, 687–692.
- 17
- 18 (10) Shi, D.; Adinolfi, V.; Comin, R.; Yuan, M.; Alarousu, E.; Buin, A.; Chen, Y.; Hoogland, S.; Rothenberger, A.; Katsiev, K.; *et al.* Low Trap-State Density and Long Carrier Diffusion in Organolead Trihalide Perovskite Single Crystals. *Science* **2015**, *347*, 519–522.
- 19
- 20 (11) Dong, Q.; Fang, Y.; Shao, Y.; Mulligan, P.; Qiu, J.; Cao, L.; Huang, J. Electron-Hole Diffusion Lengths > 175 nm in Solution-Grown CH₃NH₃PbI₃ Single Crystals. *Science* **2015**, *347*, 967–970.
- 21
- 22 (12) Zhu, H.; Fu, Y.; Meng, F.; Wu, X.; Gong, Z.; Ding, Q.; Gustafsson, M. V.; Trinh, M. T.; Jin, S.; Zhu, X.-Y. Lead Halide Perovskite Nanowire Lasers with Low Lasing Thresholds and High Quality Factors. *Nat. Mater.* **2015**, DOI: 10.1038/nmat4271.
- 23
- 24 (13) Liao, Q.; Hu, K.; Zhang, H.; Wang, X.; Yao, J.; Fu, H. Perovskite Microdisk Microlasers Self-Assembled from Solution. *Adv. Mater.* **2015**, DOI: 10.1002/adma.201500449.
- 25
- 26 (14) Stoumpos, C. C.; Frazer, L.; Clark, D. J.; Kim, Y. S.; Rhim, S. H.; Freeman, A. J.; Ketterson, J. B.; Jang, J. I.; Kanatzidis, M. G. Hybrid Germanium Iodide Perovskite Semiconductors: Active Lone Pairs, Structural Distortions, Direct and Indirect Energy Gaps, and Strong Nonlinear Optical Properties. *J. Am. Chem. Soc.* **2015**, *137*, 6804–6819.
- 27
- 28 (15) Liberman, V.; Rothschild, M.; Bakr, O. M.; Stellacci, F. Optical Limiting with Complex Plasmonic Nanoparticles. *J. Opt.* **2010**, *12*, 065001.
- 29
- 30 (16) Chong, E. Z.; Watson, T. F.; Festy, F. Autocorrelation Measurement of Femtosecond Laser Pulses Based on Two-Photon Absorption in GaP Photodiode. *Appl. Phys. Lett.* **2014**, *105*, 062111.
- 31
- 32 (17) Haske, W.; Chen, V. W.; Hales, J. M.; Dong, W.; Barlow, S.; Marder, S. R.; Perry, J. W. 65 nm Feature Sizes Using Visible Wavelength 3-D Multiphoton Lithography. *Opt. Express* **2007**, *15*, 3426–3436.
- 33
- 34 (18) Zipfel, W. R.; Williams, R. M.; Webb, W. W. Nonlinear Magic: Multiphoton Microscopy in the Biosciences. *Nat. Biotechnol.* **2003**, *21*, 1369–1377.
- 35
- 36
- 37
- 38
- 39
- 40
- 41
- 42
- 43
- 44
- 45
- 46
- 47
- 48
- 49
- 50
- 51
- 52
- 53
- 54
- 55
- 56
- 57
- 58
- 59
- 60

- 1
 - 2
 - 3
 - 4
 - 5
 - 6
 - 7
 - 8
 - 9
 - 10
 - 11
 - 12
 - 13
 - 14
 - 15
 - 16
 - 17
 - 18
 - 19
 - 20
 - 21
 - 22
 - 23
 - 24
 - 25
 - 26
 - 27
 - 28
 - 29
 - 30
 - 31
 - 32
 - 33
 - 34
 - 35
 - 36
 - 37
 - 38
 - 39
 - 40
 - 41
 - 42
 - 43
 - 44
 - 45
 - 46
 - 47
 - 48
 - 49
 - 50
 - 51
 - 52
 - 53
 - 54
 - 55
 - 56
 - 57
 - 58
 - 59
 - 60
- (19) Sheik-Bahae, M.; Said, A. A.; Wei, T.-H.; Hagan, D. J.; Van Stryland, E. W. Sensitive Measurement of Optical Nonlinearities Using a Single Beam. *Quantum Electron. IEEE J. Of* **1990**, *26*, 760–769.
- (20) Van Stryland, E. W.; Vanherzeele, H.; Woodall, M. A.; Soileau, M. J.; Smirl, A. L.; Guha, S.; Boggess, T. F. Two Photon Absorption, Nonlinear Refraction, and Optical Limiting in Semiconductors. *Opt. Eng.* **1985**, *24*, 613–623.
- (21) Van Stryland, E. W.; Woodall, M. A.; Vanherzeele, H.; Soileau, M. J. Energy Band-Gap Dependence of Two-Photon Absorption. *Opt. Lett.* **1985**, *10*, 490–492.
- (22) Sheik-Bahae, M.; Hagan, D. J.; Van Stryland, E. W. Dispersion and Band-Gap Scaling of the Electronic Kerr Effect in Solids Associated with Two-Photon Absorption. *Phys. Rev. Lett.* **1990**, *65*, 96.
- (23) DeSalvo, R.; Sheik-Bahae, M.; Said, A. A.; Hagan, D. J.; Van Stryland, E. W. Z-Scan Measurements of the Anisotropy of Nonlinear Refraction and Absorption in Crystals. *Opt. Lett.* **1993**, *18*, 194–196.
- (24) Dvorak, M. D.; Schroeder, W. A.; Andersen, D. R.; Smirl, A. L.; Wherrett, B. S. Measurement of the Anisotropy of Two-Photon Absorption Coefficients in Zincblende Semiconductors. *Quantum Electron. IEEE J. Of* **1994**, *30*, 256–268.
- (25) Hutchings, D. C.; Wherrett, B. S. Theory of Anisotropy of Two-Photon Absorption in Zinc-Blende Semiconductors. *Phys. Rev. B* **1994**, *49*, 2418.
- (26) Jishi, R. A.; Ta, O. B.; Sharif, A. A. Modeling of Lead Halide Perovskites for Photovoltaic Applications. *J. Phys. Chem. C* **2014**, *118*, 28344–28349.
- (27) Brivio, F.; Butler, K. T.; Walsh, A.; van Schilfgaarde, M. Relativistic Quasiparticle Self-Consistent Electronic Structure of Hybrid Halide Perovskite Photovoltaic Absorbers. *Phys. Rev. B* **2014**, *89*.
- (28) Giorgi, G.; Fujisawa, J.-I.; Segawa, H.; Yamashita, K. Small Photocarrier Effective Masses Featuring Ambipolar Transport in Methylammonium Lead Iodide Perovskite: A Density Functional Analysis. *J. Phys. Chem. Lett.* **2013**, *4*, 4213–4216.
- (29) Even, J.; Pedesseau, L.; Jancu, J.-M.; Katan, C. Importance of Spin-Orbit Coupling in Hybrid Organic/Inorganic Perovskites for Photovoltaic Applications. *J Phys Chem Lett* **2013**, *4*, 2999–3005.
- (30) Mosconi, E.; Amat, A.; Nazeeruddin, M. K.; Grätzel, M.; De Angelis, F. First-Principles Modeling of Mixed Halide Organometal Perovskites for Photovoltaic Applications. *J. Phys. Chem. C* **2013**, *117*, 13902–13913.
- (31) Pedesseau, L.; Jancu, J.-M.; Rolland, A.; Deleporte, E.; Katan, C.; Even, J. Electronic Properties of 2D and 3D Hybrid Organic/inorganic Perovskites for Optoelectronic and Photovoltaic Applications. *Opt. Quantum Electron.* **2014**, *46*, 1225–1232.
- (32) Hutchings, D. C.; Wherrett, B. S. Theory of the Polarization Dependence of Two-Photon Absorption in Zinc-Blende Semiconductors. *J. Mod. Opt.* **1994**, *41*, 1141–1149.
- (33) Konstantatos, G.; Clifford, J.; Levina, L.; Sargent, E. H. Sensitive Solution-Processed Visible-Wavelength Photodetectors. *Nat. Photonics* **2007**, *1*, 531–534.
- (34) Hu, X.; Zhang, X.; Liang, L.; Bao, J.; Li, S.; Yang, W.; Xie, Y. High-Performance Flexible Broadband Photodetector Based on Organolead Halide Perovskite. *Adv. Funct. Mater.* **2014**, *24*, 7373–7380.
- (35) Miller, A.; Reid, D. T. *Ultrafast Photonics*; Scottish Graduate Series; CRC Press, 2004.